Optimal strengthening of concrete plates with unidirectional fiber-reinforcing layers

Matteo Bruggi *, Alberto Taliercio

Department of Civil and Environmental Engineering, Politecnico di Milano, Piazza Leonardo da Vinci 32, 20133 Milano, Italy

Received 4 November 2014
Received in revised form 17 April 2015
Available online 6 May 2015

1. Introduction

The use of externally bonded Fiber Reinforced Polymers (FRPs), in the form of strips or sheets, to strengthen, upgrade, or retrofit deteriorated reinforced concrete or masonry structures is constantly increasing. Even limiting ourselves to consider r.c. structures, the possible fields of applications of this technique are manifold and include buildings (Garcia et al., 2010), beams (Arduini and Nanni, 1997; Norris et al., 1997; Triantafillou, 1998; Hadi, 2003; Täljsten, 2003; Pisani, 2006) and deep beams (El Maaddawy and Sherif, 2009), columns (Shahawya et al., 2000), walls (Paterson and Mitchell, 2003; Mohammed et al., 2010; Li and Lim, 2010; Li et al., 2013), bridge decks (Petrou et al., 2008; Brown and Berman, 2010), etc.

The advantages of FRPs as retrofitting materials include durability, immunity to corrosion, flexibility, low weight, high tensile strength, etc. As FRPs do not significantly increase the mass of the structural elements they are bonded to, they are preferable to classical materials, such as steel or concrete, in the repair of buildings in seismic zones. Overviews of the structural applications of FRPs in civil engineering, including retrofitting of existing buildings, can be found in Bakis et al. (2002), Van Den Einde et al. (2003) and Bai (2013).

The definition of the layout that allows the FRP layers to be used in the most effective way is still an open issue. In the presence of structural elements of simple geometry, the layout of the reinforcing layers can be defined according to engineering judgment and intuition (see e.g. Li and Lim, 2010). In the repair of windowed walls subjected in the laboratory to seismic excitation, Li et al. (2013) proposed to place the FRP strips on the damaged specimens according to a strut-and-tie scheme according to the main crack pattern. These authors showed the effectiveness of the proposed layout in recovering the mechanical performances of the walls. The idea of resorting to strut-and-tie schemes to bond FRP strips on structural elements to be retrofitted was also exploited by Krevaikas and Triantafillou (2005), who defined *a priori* a sort of mesh through which the optimal reinforcing layout has to pass.

* Corresponding author.
E-mail addresses: matteo.bruggi@polimi.it (M. Bruggi), alberto.taliercio@polimi.it (A. Taliercio).

For structural elements of complex geometry, the optimal reinforcing layout might not be reduced to a simple strut-and-tie scheme, and it would be desirable to have a general design tool available. Structural optimization, and topology optimization (TO) in particular (Bendsøe and Kikuchi, 1988), can help to define the most effective layout of the reinforcing material to be placed over any structural element, to enhance its mechanical perfor-mances upon retrofitting.

Recently, Bruggi and Taliercio (2013) proposed an approach based on TO for in-plane loaded structural elements to be retrofitted by FRPs, to define the optimal reinforcing layout that allows the maximum equivalent stress in the element to be minimized, for a prescribed amount of reinforcement. This approach was also extended to macroscopically anisotropic masonry structural elements by Bruggi et al. (2013).

Regarding the optimal reinforcement of structural elements subjected to transverse loads, most of the works available in the literature achieve this goal by adding stiffening ribs. Krog and Olhoff (1999) employed TO to define the optimal rib-reinforcement of plates subjected to static loads and free vibra-tions. A similar goal was pursued by Lam and Santhikumar (2003) through an iterative optimization procedure incorporating a num-ber of technological constraints. More recently, Ji et al. (2014) defined the optimal layout of the stiffeners by a bionic growth method. Cunha and Chaves (2014) dealt with the optimal fiber reinforcement of concrete plates subjected to lateral loads using TO. A very similar approach was used by Bruggi et al. (2014) with reference to out-of-plane loaded masonry elements. In both of these works, the anisotropy and the unsymmetric behavior in ten-sion and compression of the reinforcing layers were disregarded.

The present work deals with the optimal fiber reinforcement of two-dimensional structural elements subjected to out-of-plane loads, to be retrofitted using one of more layers of unidirectional and unilateral material. The goal is to maximize the stiffness (i.e., to minimize the elastic compliance) of the reinforced plate, for a given amount of reinforcement. Strain energy is adopted as objective function, in full agreement with prescriptions of technical codes for load path recovery, see in particular EC2 (2004) and ACI 318 (2002). Differences between energy-based and stress-based topology optimization have been thoroughly investigated in the literature. Readers are referred in particular to Duysinx and Bendsøe (1998) and Rozvany (1998) for comparisons of volume-constrained compliance minimization versus stress-constrained volume minimization, and to Li et al. (1999) for a discussion on the equivalence between the stress criterion and the stiffness one within the field of evolutionary structural optimization.

The layout of the paper is as follows. First (Section 2), the equations governing the linear elastic behavior of homogeneous isotropic plates reinforced by FRP layers and obeying the Kirchhoff–Love model are recalled. The elastic properties of the reinforcing material are assumed to depend locally on the material density. Then (Section 3), the topology optimization problem is formulated: the structural stiffness is maximized for a given amount of the reinforcement, by suitably selecting its local arrangement and orientation, which are both assumed to be design variables. Compressive stresses along the reinforcing fibers are avoided adding further constraints. A number of numerical applications are presented in Section 4 to illustrate the capabilities of the proposed approach: the possibility of taking cracking of the r.c. plate into account is also covered in the model, as well as the case where the extrados of the plate is not accessible. The obtained optimal reinforcement layouts are found to effectively resist the failure mechanisms that limit analysis of the unreinforced plates would predict. Finally, the salient features of the proposed approach and the main findings of the study are summarized in Section 5, where future perspectives of the research are also outlined.

2. Equations governing the elastic equilibrium of a reinforced plate

Consider a thin concrete plate of constant thickness, whose mid-plane occupies a domain A in the plane (x_1, x_2) of a Cartesian orthogonal reference system $Ox_1x_2x_3$. Concrete is assumed to behave as a homogeneous isotropic linear elastic material. The plate is subjected to transverse loads, acting along x_3. Reinforcing layers are applied on selected regions of both sides of the plate, with the aim of improving its overall stiffness: let K be the total number of reinforcing layers. The layers are supposed to consist of a unidirectional FRP, which behaves macroscopically as a linear elastic orthotropic material. These layers add bending stiffness to the plate thanks to their internal lever arm.

The reinforced plate is assumed to obey the Kirchhoff–Love model, which implies that the reinforcing layers are perfectly bonded to the concrete core. Let $\underline{\chi} = [\chi_{xx}\, \chi_{yy}\, \chi_{xy}]^T$ and $\underline{M} = [M_{xx}\, M_{yy}\, M_{xy}]^T$ be the arrays gathering the Cartesian components of the mid-plane curvatures and of the moments about the mid-plane, respectively. Also, let $\underline{\varepsilon} = [\varepsilon_{xx}\, \varepsilon_{yy}\, 2\varepsilon_{xy}]^T$ be the array gathering the non-vanishing strain components at any point of the plate. According to Kirchhoff–Love plate model, $\underline{\varepsilon} = x_3\underline{\chi}$.

The array of the Cartesian stress components in the concrete plate $\underline{\sigma}^c = [\sigma^c_{11}\, \sigma^c_{22}\, \sigma^c_{12}]^T$ can be written as $\underline{\sigma}^c = \mathbf{C}^c\underline{\varepsilon}$, with:

$$\mathbf{C}^c = \frac{E^c}{(1+\nu^c)(1-\nu^c)} \begin{bmatrix} 1 & \nu^c & 0 \\ \nu^c & E^c & 0 \\ 0 & 0 & (1-\nu^c)/2 \end{bmatrix}, \tag{1}$$

where E^c and ν^c are the Young's modulus and the Poisson's ratio of plain concrete, respectively.

The reinforcing material is assumed to exhibit prevailing stiffness along one direction, as is the case of unidirectional FRPs. Accordingly, the elastic constants are assumed to vanish but for the Young modulus along the fiber direction E^f. Let X_{1k} and X_{2k} be a couple of orthogonal Cartesian axes in the plane (x_1, x_2), with X_{1k} locally aligned with the reinforcing fibers in the kth layer and forming an angle θ_k with the Cartesian axis x_1 (see Fig. 1). In principle, $\theta_k = \theta_k(x_1, x_2)$. Let the stress components in the kth reinforcing layer be collected in an array $\underset{k}{\underline{\tilde{\sigma}}^f} = [\tilde{\sigma}^f_{11}\, \tilde{\sigma}^f_{22}\, \tilde{\sigma}^f_{12}]^T_k$: a tilde denotes quantities referred to the symmetry axes of the lamina,

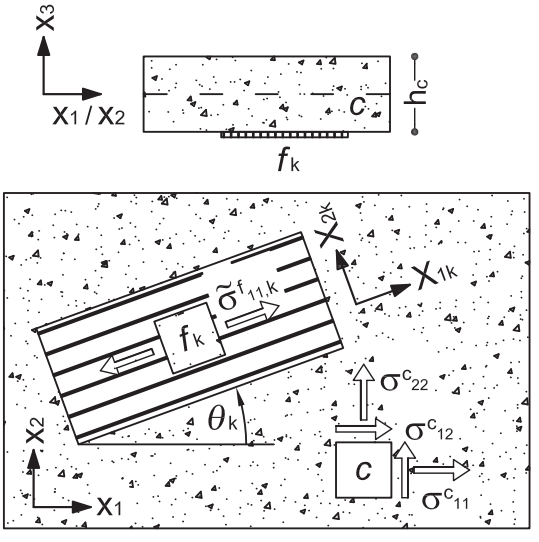

Fig. 1. Part of a concrete plate (c) retrofitted with a unidirectional fiber-reinforced layer (f, k).

X_{1k} and X_{2k}. The only non-vanishing stress component in the reinforcement is $\widetilde{\sigma}^f_{11,k}$. The fiber-reinforcement is therefore modeled as set of two-dimensional layers, each one working as a spring, since it is able to carry only axial loads along the fibers.

A suitable penalization procedure will be implemented in Section 3 to ensure that the reinforcement acts as a tension-only material (i.e. $\widetilde{\sigma}^f_{11,k} > 0 \ \forall k$). This is consistent with the poor mechanical performances of a thin lamina in compression: because of their negligible stiffness under compressive loads and the inherent risk of buckling phenomena, fiber-reinforced strips are employed as distributed ties that strengthen any brittle structure against potential cracking and tensile failure.

K normalized density fields $0 \leqslant \rho_k \leqslant 1$ are defined over the whole domain A, in order to determine whether the kth reinforcing layer is applied at any point of the plate ($\rho_k = 1$) or not ($\rho_k = 0$). In order to avoid numerical instabilities resulting from a pure black-or-white design, according to the so-called Solid Isotropic Material with Penalization (SIMP) model (Bendsøe and Kikuchi, 1988; Eschenauer and Olhoff, 2001; Bendsøe and Sigmund, 2003), the stiffness of the FRP layers is assumed to depend on ρ_k through a power law. Thus, the elasticity matrix of the reinforcing material in the local reference system of the kth layer can be expressed as $\mathbf{C}^f_k = \rho^p_k \mathbf{C}^{f0}$, with

$$\mathbf{C}^{f0} = \begin{bmatrix} E^f & 0 & 0 \\ 0 & 0 & 0 \\ 0 & 0 & 0 \end{bmatrix} \tag{2}$$

In the numerical simulations presented in Section 4 p is taken equal to 3, following the suggestions found in the literature (Bendsøe and Sigmund, 1999).

Let $\underline{\sigma}^f_k = [\sigma^f_{11}\ \sigma^f_{22}\ \sigma^f_{12}]^T_k$ be the array of the Cartesian stress components in any one of the reinforcing layers referred to the global axes x_1, x_2. $\underline{\sigma}^f_k$ is given by $\underline{\sigma}^f_k = \mathbf{T}_k(\theta_k)\widetilde{\underline{\sigma}}^f_k$, where $\mathbf{T}_k$ is a transformation matrix given by

$$\mathbf{T}_k = \begin{bmatrix} c_k^2 & s_k^2 & -2c_k s_k \\ s_k^2 & c_k^2 & 2c_k s_k \\ c_k s_k & -c_k s_k & c_k^2 - s_k^2 \end{bmatrix}, \tag{3}$$

where $c_k = \cos\theta_k$ and $s_k = \sin\theta_k$. Accordingly, the stress-strain law for each reinforcing layer in the global reference system can be written as

$$\underline{\sigma}^f_k = \rho^p_k \mathbf{T}_\mathbf{k}(\theta_k)\mathbf{C}^{f0}\mathbf{T}^T_\mathbf{k}(\theta_k)\underline{\varepsilon}. \tag{4}$$

Denote by h_c the thickness of the concrete plate: the intrados of the plate is assumed to be the side $x_3 = -h_c/2$, and the extrados to be the side $x_3 = +h_c/2$. Also, denote by h_{fk} the thickness of any reinforcing layer, k. The moment array is given by:

$$\underline{M} = \int_{-h_c/2}^{h_c/2} \underline{\sigma}^c x_3 dx_3 + \sum_{k=1}^{K} \int_{z_k}^{z_k+h_{fk}} \underline{\sigma}^f_k x_3 dx_3, \tag{5}$$

where z_k is the applicate of the intrados of the kth layer; denoting by K_{in} (respectively, by K_{ex}) the number of layers at the intrados (resp., at the extrados) of the plate, $z_1 = -(h_c/2 + \sum_{k=1}^{K_{in}} h_{fk})$ and $z_K = h_c/2 + \sum_{k=K_{in}+1}^{K_{ex}} h_{fk}$, with $K_{in} + K_{ex} = K$ and $K_{in}, K_{ex} \geqslant 1$. This formulation includes the possibility that overlapping unidirectional strips are placed at either side of the plate, as is often required for an effective reinforcement of two-way plates by FRPs. If both sides of the plate are accessible, at least two layers per side can be optimized ($K \geq 4$), whereas $K \geq 2$ if one side (usually, the intrados) can be reinforced.

Exploiting the stress–strain relations in Eqs. (1) and (4) and recalling that $\underline{\varepsilon} = x_3\underline{\chi}$, one gets the moment-curvature law for the reinforced plate:

$$\underline{M} = \left(\int_{-h_c/2}^{h_c/2} \mathbf{C}^c x_3^2 dx_3 + \sum_{k=1}^{K} \int_{z_k}^{z_k+h_{fk}} \rho^p_k \mathbf{T}_k(\theta_k)\mathbf{C}^{f0}\mathbf{T}^T_k(\theta_k) x_3^2 dx_3 \right) \underline{\chi}. \tag{6}$$

As the FRP layers are usually much thinner than the concrete core (i.e. $z_k \approx \pm h_c/2, \forall k$), in the manipulation of Eq. (6) higher order terms can be neglected and the simplified $\underline{M}$–$\underline{\chi}$ law reads:

$$\begin{aligned} \underline{M} &= \frac{h_c^3}{12}\mathbf{C}^c\underline{\chi} + \left(\frac{h_c}{2}\right)^2 \left(\sum_{k=1}^{K} \rho^p_k \mathbf{T}_k(\theta_k)\mathbf{C}^{f0}\mathbf{T}^T_k(\theta_k) h_{fk} \right) \underline{\chi} \\ &= \underline{M}^c + \underline{M}^f(\boldsymbol{\rho}, \boldsymbol{\theta}). \end{aligned} \tag{7}$$

Here $\underline{M}^c$ denotes the moment acting in the concrete plate, whereas $\underline{M}^f$ is the part of the moment carried by the FRP layers, which explicitly depends on the design variables, gathered in two arrays of K entries, $\boldsymbol{\rho}$ and $\boldsymbol{\theta}$.

The implementation of the theoretical formulation described above into a finite element code is straightforward. Assuming perfect bonding between the layers, any reinforcing layer can be modeled as an additional in-plane stiffness contribution to the underlying plate. Four node elements for thin plates obeying Kirchhoff–Love theory can be adopted to model the isotropic concrete plate of thickness h_c. On the same mesh, the stiffness of a set of four node plane stress elements can be added for each orthotropic reinforcing layer at the extrados or at the intrados of the plate, with an offset of $+h_c/2$ or $-h_c/2$, respectively, along x_3 – see Fig. 1. Section 3.1 provides additional details on the resulting element stiffness matrix to model the composite structure through a two-dimensional finite element mesh.

According to Eq. (7), twice the strain energy, Ω, stored in a reinforced plate subject to a curvature field $\underline{\chi}$ is given by:

$$\begin{aligned} 2\Omega(\boldsymbol{\rho}, \boldsymbol{\theta}) &= \int_A \underline{M}^T \underline{\chi} dx_1 dx_2 \\ &= I_c \int_A \underline{\chi}^T \mathbf{C}^c \underline{\chi} dx_1 dx_2 + \left(\frac{h_c}{2}\right)^2 \\ &\quad \times \int_A \underline{\chi}^T \left(\sum_{k=1}^{K} \rho^p_k \mathbf{T}_k(\theta_k)\mathbf{C}^{f0}\mathbf{T}^T_k(\theta_k) h_{fk} \right) \underline{\chi} dx_1 dx_2. \end{aligned} \tag{8}$$

where where $I_c = h_c^3/12$ is the moment of inertia of the concrete section. As anticipated in Section 1, the search for the optimal distribution of fiber-reinforcement to be applied on a concrete plate is performed according to an energy-based criterion. The stiffness of the reinforced plate is maximized by minimizing the functional in Eq. (8). For a realistic treatment of the problem, the possibility of cracking of the concrete core has to be taken into account. To do this, a simple strategy is suggested by provisions of technical codes when computing deflections, see ACI 318 (2002) and Gilbert (1999). The reduction in flexural stiffness due to cracking is accounted for by replacing in Eq. (8) the gross moment of inertia I_c of the concrete plate by a reduced effective moment of inertia I_e, which reads:

$$I_e = \left(\frac{M_{cr}}{M_a}\right)^3 I_c + \left[1 - \left(\frac{M_{cr}}{M_a}\right)^3\right] I_{cr}, \tag{9}$$

where I_{cr} the moment of inertia of the cracked section, M_a the moment computed through a linear elastic analysis and M_{cr} the cracking moment. One may therefore perform a preliminary analysis of the unreinforced plate with the gross moment of inertia, and then start the optimization procedure with the reduced moment of Eq. (9).

3. Problem formulation

3.1. Constrained minimization of the structural compliance

A topology optimization approach for the distribution of tension-only unidirectional reinforcement is herein investigated to retrofit concrete plates, following the approach originally proposed in Bruggi and Taliercio (2013) for in-plane loaded two-dimensional structural elements.

As recalled in Section 1, in the literature several works can be found which address the automatic generation of reinforcement layouts for structural elements. A classical application exploits topology optimization to derive truss-like structures, the tensile members of which can be interpreted as load paths along which rebars have to be placed in concrete elements, see in particular Liang et al. (2000, 2001) and Victoria et al. (2011). Building codes suggest to adopt the strain energy stored in the structural element as a suitable objective function to generate feasible layouts at the ultimate limit state, see also Bruggi (2010). The minimization of the strain energy for the application of FRP reinforcements to existing in-plane loaded structural elements has been implemented accordingly in Pedersen (1989), Cheng and Kikuchi (1994) and Bruggi and Taliercio (2013).

Here, a strengthening strategy is proposed for concrete plates subjected to out-of-plane loads based on a minimum compliance formulation to distribute a prescribed amount of unidirectional tension-only reinforcement over its sides. The objective function is the so-called compliance $\mathcal{C}$, that is, twice the strain energy of the reinforced structure, see Eq. (8). The constrained minimization of $\mathcal{C}$ will be performed using the Finite Element Method in its displacement-based formulation. Four-node 2D finite elements will be used. Let N be the number of finite elements into which the reinforced structure is subdivided and let $\mathbf{U}_i$ denote the array of the twelve unknown degrees of freedom of the ith finite element. Following a conventional scheme in topology optimization, one density unknown $\rho_{i,k}$ and one orientation unknown $\theta_{i,k}$ are defined for each one of the K reinforcing layers to be placed over any side of the ith element, for a total of $2N \cdot K$ design variables. The stiffness stiffness matrix of the ith reinforced finite element can be therefore written as:

$$\mathbf{K}_i(\boldsymbol{\rho}_i, \boldsymbol{\theta}_i) = \mathbf{K}_i^c + \sum_{k=1}^{K} \rho_{i,k}^p \mathbf{K}_{i,k}^f(\theta_{i,k}), \tag{10}$$

where $\boldsymbol{\rho}_i$ and $\boldsymbol{\theta}_i$ are two arrays of K entries each, gathering the design variables of all the layers reinforcing the element, $\mathbf{K}_i^c$ is the stiffness contribution of the underlying concrete slab, whereas $\rho_{i,k}^p \mathbf{K}_{i,k}^f(\theta_{i,k})$ accounts for the kth unidirectional reinforcing layer arranged at either side of the concrete element. Denoting by $\mathbf{B}_i$ the compliance matrix of the ith finite element, which allows the curvatures in the element to be expressed as $\underline{\chi} = \mathbf{B}_i \mathbf{U}_i$, the two stiffness matrices $\mathbf{K}_i^c$ and $\mathbf{K}_{i,k}^f$ are given by

$$\begin{aligned} \mathbf{K}_i^c &= I_e \int_{A_i} (\mathbf{B}_i)^T \mathbf{C}^c \mathbf{B}_i dx_1 dx_2, \\ \mathbf{K}_{i,k}^f &= \frac{h_c^2}{4} h_{fk} \int_{A_i} (\mathbf{B}_i)^T \mathbf{T}_k \mathbf{C}^{f0} \mathbf{T}_k^T \mathbf{B}_i dx_1 dx_2, \end{aligned} \tag{11}$$

being A_i the area of the element.

In the minimization of the (discretized) structural compliance, the reinforcement will be prescribed not to exceed a given fraction, V_f, of the total volume of the plate. Also, the stress along the fibers in the kth reinforcing layer of the ith finite element, $\widetilde{\sigma}_{i,k}^f$, will be prescribed to be non-negative. Accordingly, the discrete version of the constrained minimization problem reads:

$$\begin{cases} \min\limits_{\rho_{i,k}, \theta_{i,k}} & \mathcal{C} = \sum\limits_{i=1}^{N} \mathbf{U}_i^T \mathbf{K}(\rho_{i,k}, \theta_{i,k}) \mathbf{U}_i \\ \text{s.t.} & \sum_{i=1}^{N} \left[\mathbf{K}_i^c + \sum\limits_{k=1}^{K} \rho_{i,k}^p \mathbf{K}_{i,k}^f(\theta_{i,k}) \right] \mathbf{U} = \mathbf{F}, \\ & \sum_{k=1}^{K} \sum\limits_{i=1}^{N} \rho_{i,k} A_i \Big/ \sum\limits_{i=1}^{N} 2A_i \leqslant V_f, \\ & \widetilde{\sigma}_{i,k}^f(\rho_{i,k}, \theta_{i,k}) \geqslant 0, \quad \text{for} \quad i = 1, \ldots, N \quad k = 1, \ldots, K \\ & 0 \leqslant \rho_{i,k} \leqslant 1, \\ & 0 \leqslant \theta_{i,k} < \pi. \end{cases} \tag{12}$$

The first constraint of the optimization problem in Eq. (12) enforces the equilibrium for the reinforced structural element in weak form: the global stiffness matrix is split into two contributions related to the underlying concrete element and the reinforcing layers, in agreement with Eq. (10). The second constraint prescribes the maximum allowable amount of reinforcing material. The third constraint avoids compressive stresses along the fibers in the FRP layers. Finally, Eqs. (12).5 and (12).6 define bound constraints for the two sets of design variables.

3.2. Implementation

In principle, the stress constraints prescribed by Eq. (12).4 have to be enforced all over the domain A for each one of the available reinforcing layers, thus requiring a CPU-demanding algorithm when implemented. Additionally, the thickness of any reinforcement layer is allowed to vanish, see Eq. (12).5, meaning that a singularity problem for the stress in the reinforcement is expected to arise, see e.g. Cheng and Guo (1997).

Resorting to the penalization scheme adopted by Ananiev (2005) and Bruggi (2014) to deal with unilateral materials, one can get rid of possible compressive stresses along the fibers in the optimal design, without implementing any local enforcement on the stress field. This turns the multi-constrained formulation into a more effi-cient volume-constrained problem, which can be efficiently solved through the Method of Moving Asymptotes (Svanberg, 1987).

The adjoint method is adopted for the fast computation of the sensitivities of the objective function, see in particular Bendsøe et al. (1985), Haftka and Gürdal (1992) and Bendsøe and Sigmund (2003). At each step of the iterative minimization procedure, some modified densities $\widehat{\rho}_{i,k}$ are introduced for a straightforward computation of a reduced compliance $\widehat{\mathcal{C}}$, in which the terms related to tensile stresses along the fibers are penalized; the relevant sensitivities are modified accordingly. The modified densities are defined as:

$$\begin{cases} \widehat{\rho}_{i,k} = \rho_{i,k}, & \text{if } \widetilde{\sigma}_{i,k}^f(\rho_{i,k}, \theta_{i,k}) \geqslant 0, \\ \widehat{\rho}_{i,k} = \alpha \rho_{i,k}, & \text{otherwise} \end{cases} \tag{13}$$

($k = 1, \ldots, K, i = \ldots, N$), where $\alpha \in]0, 1[$ is a penalization parameter that is herein assumed equal to 0.5, see Ananiev (2005). According to Eq. (12).1 the reduced compliance is computed as:

$$\widehat{\mathcal{C}} = \sum_{i=1}^{N} \mathbf{U}_i^T \mathbf{K}(\widehat{\rho}_{i,k}, \theta_{i,k}) \mathbf{U}_i. \tag{14}$$

The sensitivity of the reduced objective function $\widehat{\mathcal{C}}$ with respect to the modified density $\widehat{\rho}_{i,k}$ referring to the kth layer and the ith element reads:

$$\frac{\partial \widehat{\mathcal{C}}}{\partial \widehat{\rho}_{i,k}} = p \widehat{\rho}_{i,k}{}^{(p-1)} \mathbf{U}_i^T \mathbf{K}_{i,k}^f(\theta_{i,k}) \mathbf{U}_i, \tag{15}$$

whereas the sensitivity with respect to the orientation $\theta_{i,k}$ referring to the kth layer and the ith element reads:

$$\frac{\partial \widehat{\mathcal{C}}}{\partial \theta_{i,k}} = \widehat{\rho}_{i,k}\, {}^{p}\mathbf{U}_i^T \frac{\partial}{\partial \theta_{i,k}} \mathbf{K}_{i,k}^f(\theta_{i,k}) \mathbf{U}_i. \tag{16}$$

The reduced compliance and the relevant sensitivities are passed to the minimizer, which iteratively searches for a new updated set of variables $\widehat{\rho}_{i,k}$, which allow the real densities $\rho_{i,k}$ to be also updated, see Bruggi (2014) for details. The above procedure is repeated until convergence is attained, i.e. any change in the values of the minimization unknowns at two subsequent iterations is less than a given tolerance (10^{-3} in the numerical applications of Section 4).

4. Numerical investigations

A few examples are presented in this section to assess the capabilities of the proposed numerical procedure and to investigate the features of the achieved optimal layouts. In all the examples, a reinforced concrete plate with a thickness $h_c = 0.3$ m, either L-shaped or square, is considered. A concrete class C20/25 is assumed. The original reinforcement existing in the plate is made of $5\phi14$ steel B450C bars per unit length parallel to the sides of the plate and placed both at the intrados and at the extrados, with a cover of 30 mm. The adopted elastic modulus for concrete is $E_c = 25,000$ MPa, whereas the tensile strength in bending is $f_{cfm} = 1.35$ MPa. Both values are lower than those prescribed by codes for new buildings, to account for possible deterioration effects of concrete in the structure.

With the above material and geometrical parameters, the ultimate bending moment of the section, M_u, is approximately of 80 kNm/m, the cracking moment M_{cr} is ≈ 20 kNm/m, and the ratio of the gross moment of inertia to the reduced moment of inertia I_e/I_c is $\approx 1/3$.

Let us assume that the plate has to be repaired, with the main goal of relieving tensile stresses in the rebars. This may be required, for instance, because of some corrosion taking place in the steel reinforcement, as a consequence of chloride attack or a carbonation process. Retrofitting is operated removing both dead and live loads (e.g. raising the deck on hydraulic jacks or jackscrews), applying the FRP strips and then reloading as in the original scenario. The term "length" refers hereafter to the size of the unidirectional FRP strips parallel to the fibers.

In all the simulations presented hereafter, the plate is assumed to be subjected to a uniformly distributed load of 12 kN/m^2. The maximum allowable volume fraction of reinforcement is $V_f = 0.5$. The number of available reinforcing layers is $K = 4$, meaning that both sides of the slab are accessible to apply FRP strips. Any change in these default values will be explicitly stated in the text.

The formulation in Eq. (12) is implemented to maximize the overall stiffness of the retrofitted subjected to the design loads. Maximum deflections and principal moments acting in the unreinforced plate and in the reinforced concrete layer of the optimally-strengthened plate are reported, to compare the ex-ante and ex-post performances of the structures. The effect of cracking is also taken into account through the penalization of the moment of inertia of the sections according to Eq. (9). The values obtained in the four examples described hereafter are summarized in Table 1: v_u and v_r denote the maximum deflection in the unreinforced and in the reinforced plate, respectively; $M^c_{+,u}$ (respectively, $M^c_{-,u}$) denotes the absolute value of the maximum sagging (resp., hogging) principal moment in the unreinforced plate, whereas $M^c_{+,r}$ (resp., $M^c_{-,r}$) denotes the corresponding moment in the reinforced plate.

4.1. Example 1. Clamped L-shaped plate

4.1.1. Uncracked plate

The first example addresses the L-shaped plate shown in Fig. 2(1), which is fully clamped along the longest edges, $\overline{AB}$ and

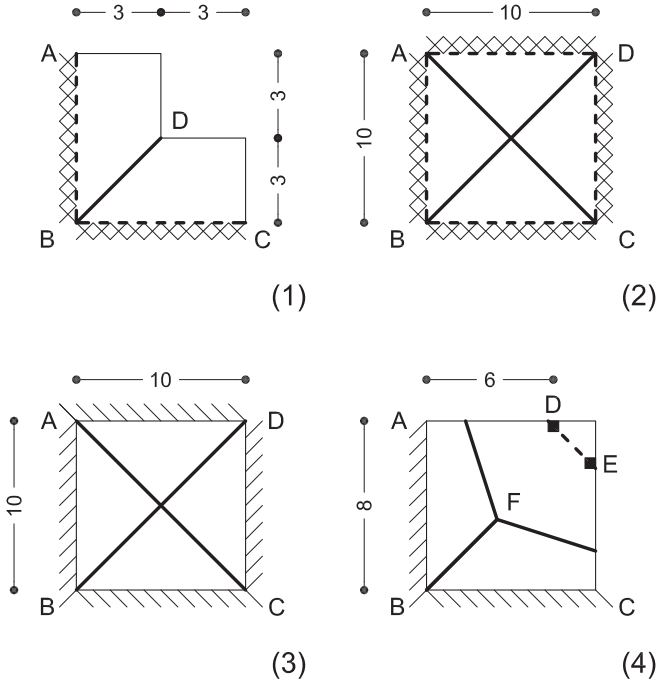

Fig. 2. Examples 1–4. Geometry, boundary conditions and simplified yield line patterns. Dimensions are in m. The symbol/stands for simply supported edges, whereas × denotes clamped edges. Thick solid lines correspond to sagging (positive) yield lines, whereas thick dashed lines denote hogging (negative) yield lines.

Table 1
Examples 1–4. Unreinforced ($_u$) versus reinforced ($_r$) plate: comparison in terms of maximum deflection v and maximum moments in the concrete layer inducing tensile stresses at the extrados M^c_- (hogging moment) and at the intrados M^c_+ (sagging moment).

Example (label)	Account for cracking	Figure (number)	v_u mm	$M^c_{-,u}$ kNm/m	$M^c_{+,u}$ kNm/m	v_r mm	$M^c_{-,r}$ kNm/m	$M^c_{+,r}$ kNm/m
1	no	5	1.70	47.20	24.20	1.58	43.52	22.17
	yes	9	2.78	40.38	26.18	2.43	32.57	22.89
	yes	10	2.78	40.38	26.18	2.41	32.46	22.94
	yes	11	2.78	40.38	26.18	2.48	33.42	23.32
2	no		2.58	53.65	25.33			
	yes	15	3.96	38.79	26.83	3.54	33.09	23.97
3	no		8.27	43.77	52.95			
	yes	21	22.59	45.43	51.79	20.19	36.86	45.91
4	no		3.29	147.59	41.75			
	yes	24	7.43	114.82	41.90	6.38	90.43	35.94
	yes	26	7.43	114.82	41.90	6.65	106.74	37.11

$\overline{BC}$. A preliminary finite element analysis is performed under the effect of the distributed load to compute the principal moments in the concrete plate assumed to be uncracked. Fig. 3 shows the relevant principal directions, which are marked in red in case of sagging (positive) moments, or in blue in the case of hogging (negative) moments. The length of the vectors is proportional to the modulus of the principal moments M_I and M_{II}, the contours of which are represented in Figs. 4(a) and (b), respectively, being $M_I \leqslant M_{II}$. The maximum values of the deflection and of the principal moments in the uncracked plate are reported in the first line of Table 1. The maximum negative (hogging) moment is found at the points A and C of Fig. 2(1), whereas the maximum positive (sagging) moment is attained at point D.

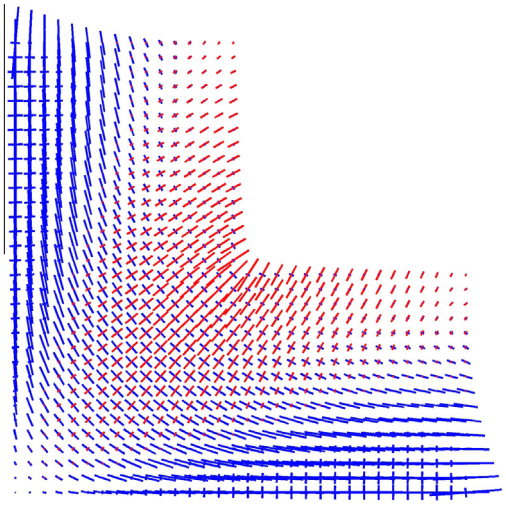

Fig. 3. Example 1. Principal moment directions in the unreinforced uncracked concrete slab. Red vectors stand for sagging (positive) moments, whereas blue vectors stand for hogging (negative) moments. (For interpretation of the references to color in this figure legend, the reader is referred to the web version of this article.)

A first numerical investigation is performed through Eq. (12) neglecting the effect of cracking, that is, preserving the gross moments of inertia I_c of the concrete core all over the domain within the optimization procedure. The achieved optimal design is presented in Figs. 5(a) and (b), showing the optimal layout of the reinforcement at the extrados and at the intrados, respectively. The optimal direction of the FRP strips is represented through vec-torial plots of the principal stresses in the layers at the extrados (Fig. 6(a)) and at the intrados (Fig. 6(b)) of the plate. The optimiza-tion procedure distributes most of the available amount of reinforcement in the regions at the extrados where the highest negative moments are found, which means along the edges $\overline{AB}$ and $\overline{BC}$, except for the region around the outer corner B. The remaining part of reinforcement is distributed at intrados in the region of maximum positive moment, i.e. around the inner corner D. The directions of the fibers are perpendicular to the principal moment directions. Hence, the unilateral reinforcement is aligned with the directions of the highest tensile principal stresses at either

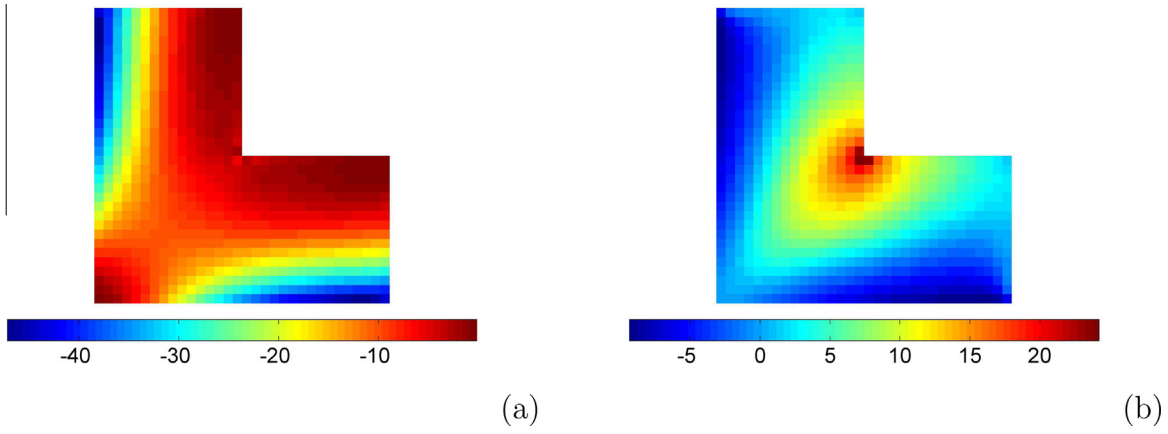

Fig. 4. Example 1. Principal moments in the unreinforced uncracked concrete slab: M_I(a) and M_{II}(b), with $M_I \leqslant M_{II}$.

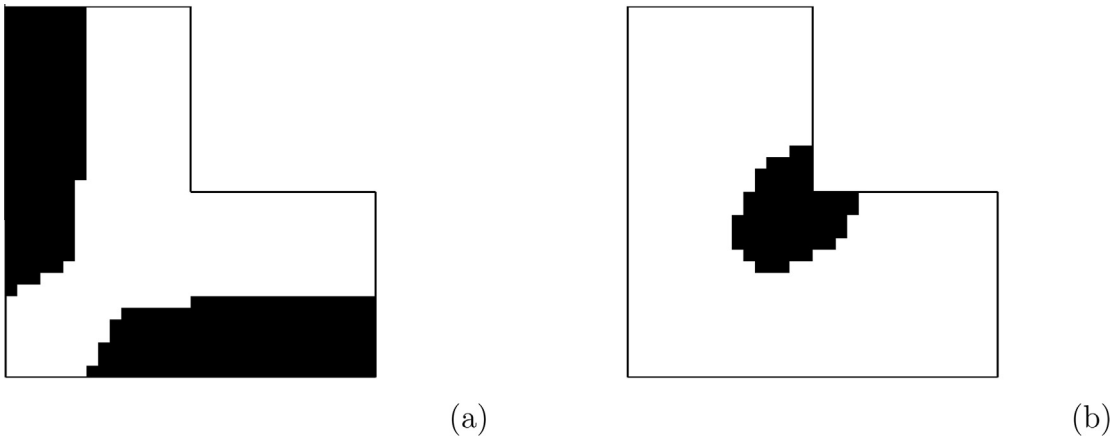

Fig. 5. Example 1. Optimal layout of the reinforcement for the uncracked slab: extrados (a) and intrados (b).

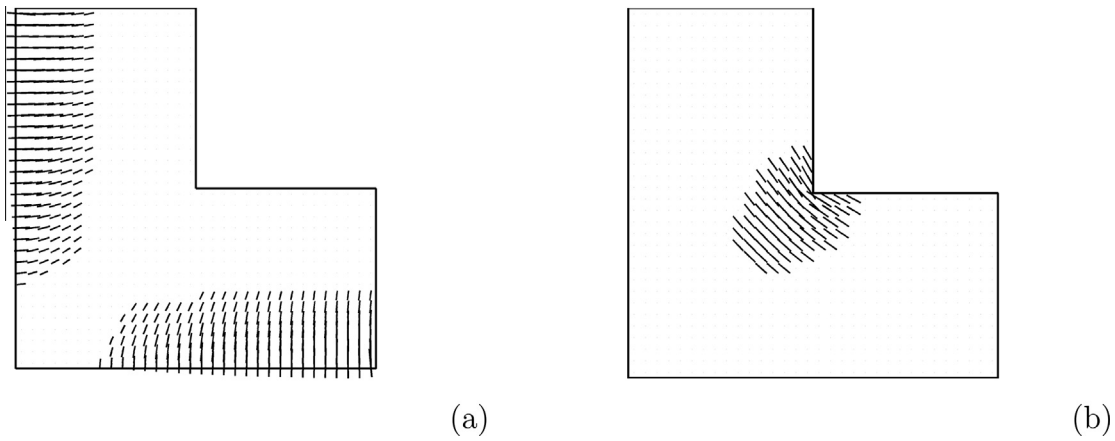

Fig. 6. Example 1. Optimal orientation of the fibers in the reinforcement of Fig. 5 for the uncracked slab: extrados (a) and intrados (b).

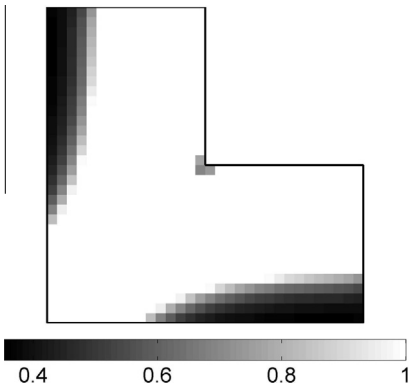

Fig. 7. Example 1. Ratio I_c/I_e accounting for cracking in the concrete slab.

side of the plate. No compressive stress is found in the fibers, as required by the constrained optimization procedure.

The first line of Table 1 shows the effectiveness of the strain energy plate as objective function in designing reinforcement patterns that increase the overall stiffness of the plate (see v_r/v_u) while decreasing the maximum moments in the concrete layer (see $M^c_{-,r}/M^c_{-,u}$ and $M^c_{+,r}/M^c_{+,u}$). More demanding multi-constrained formulations could be implemented to control moment peaks following e.g. Bruggi and Taliercio (2013) and Bruggi and Duysinx (2013).

The obtained reinforcement layout can be easily implemented in practice, as the orientation of the fibers which define the strip directions is almost piecewise uniform. It is interesting to point out that fibers are distributed so as to cross the yield lines characterizing the collapse mechanism predicted by plastic design, see in particular Johansen (1962) and Kennedy and Goodchild (2003). According to limit analysis theory, a suitable set of mechanisms consisting of rigid blocks and plastic hinges can be defined and the mechanism corresponds to the minimum activation load can be pinpointed. Fig. 2(1) shows the two hogging lines $\overline{AB}$ and $\overline{BC}$ along with the sagging line $\overline{BD}$ of the collapse mechanism of the plate. Comparing this sketch with the orientation of the reinforcing fibers in Fig. 6, one can easily check that both families of lines are crossed almost perpendicularly by the fibers at both sides of the plate.

4.1.2. Cracked plate

The effect of cracking in the achievement of the optimal reinforcement is investigated following the approach described in Section 2. Fig. 7 shows the ratio of the reduced effective moment of inertia I_e to the gross moment of inertia I_c of the concrete core, computed according to Eq. (9). This element-wise distribution of I_e is used to perform the finite element analysis required by Eq. (12) to distribute the prescribed maximum amount of fiber-reinforcement and minimize the strain energy of the cracked plate. Fig. 8 provides plots of the principal moments computed from a post-processing of the analysis of the cracked plate, which can be

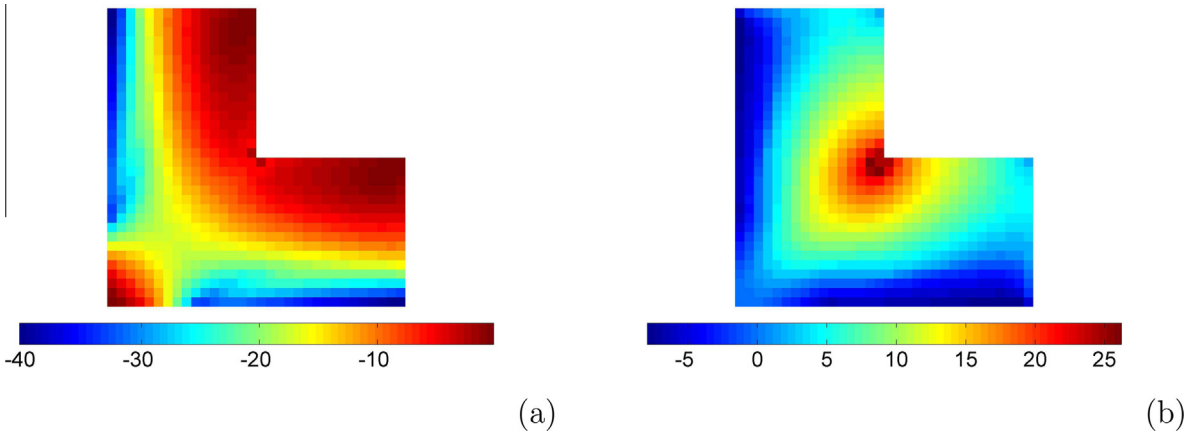

Fig. 8. Example 1. Principal moments in the unreinforced cracked concrete slab: M_I(a) and M_{II}(b), with $M_I \leqslant M_{II}$.

compared with the relevant patterns referring to the uncracked structure, shown in Fig. 4. A remarkable decrease in terms of maximum negative moment $M^c_{-,u}$ is observed (see also the second line of Table 1), and highly stressed regions extend nearly over all the clamped edges at the extrados, except corner *C*. Conversely, the maximum positive moment $M^c_{+,u}$ slightly increases, mainly due to the loss in bending stiffness along the restrained edges.

The achieved optimal layout accounting for the reduced inertia is shown in Fig. 9. Notwithstanding the increased value of $M^c_{+,u}$, a slight reduction in the amount of reinforcement compared to the case in which concrete is uncracked (Fig. 6) is paid at the intrados to achieve an improved layout at the extrados. The length of the strips at the extrados is reduced in the vicinity of the clamped edges (especially near points *A* and *C*) in order to strengthen the corner region through a set of 45-degrees strips. As in the previous case, fibers are almost perpendicular to the directions of the prin-cipal moments at both sides. According to the second line of Table 1, the achieved layout allows the maximum moments to sig-nificantly decrease (of about 20% in case of M^c_-), whereas compli-ances decreases of more than 12%.

A final assessment of the proposed formulation addresses the influence of the amount of FRP on the optimal reinforcement layout. Eq. (12) implements a classical volume-constrained minimization where the volume fraction of available reinforcement is prescribed, herein $V_f = 0.5$. Fig. 10 shows the optimal design assuming $V_f = 0.75$: basically, the same layout of Fig. 9 is obtained, with an increased length of the reinforcing strips both at the extrados and at the intrados. Fig. 11 provides the optimal design assuming $V_f = 0.25$: in this case, the allowed amount of strengthening material is extremely low, and the distribution of reinforcing strips at both sides of the plate matches the layout shown in Fig. 9 only in limited regions. The third line of Table 1 shows that only a minimum increase in terms of mechanical performances (displacements and moments in the reinforced plates) is achieved adopting the greater amount of reinforcement, whereas a slightly more remarkable decrease is found for the lower amount of reinforcement (see the fourth line of Table 1). According to these remarks, taking $V_f = 0.5$ seems to be a reasonable compromise between costs and benefits for a preliminary design of the reinforcement. Alternatively, an approach based on the so-called "performance index" (Liang and Steven, 2002) could be used, in which several performances of the design domain can be enhanced using a sort of multi-objective optimization (e.g., in terms of amount of reinforcement and overall stiffness), see also Liang et al. (1999). Note, however, that an optimization approach based on linear elasticity defines only the topology and the orientation of the reinforcement: the real amount of reinforcement has to be determined according to an ultimate limit state analysis, taking into account the prescriptions of technical codes, such as the anchorage length (see Chen and Teng, 2001).

A direct comparison of Figs. 6 and 9 suggests that cracking can remarkably affect the optimal distribution of unilateral reinforcement. Accordingly, all the numerical investigations described in

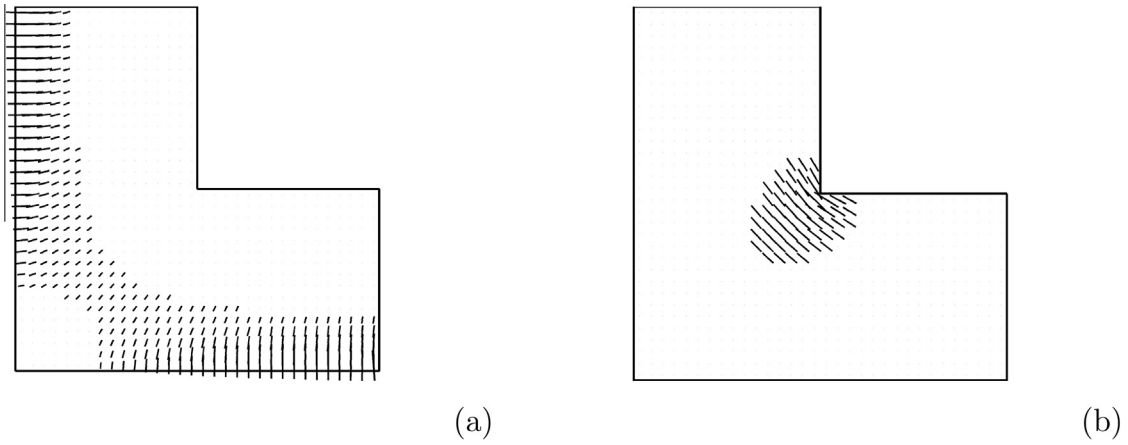

Fig. 9. Example 1. Optimal topology and orientation of the reinforcement for the cracked slab: extrados (a) and intrados (b).

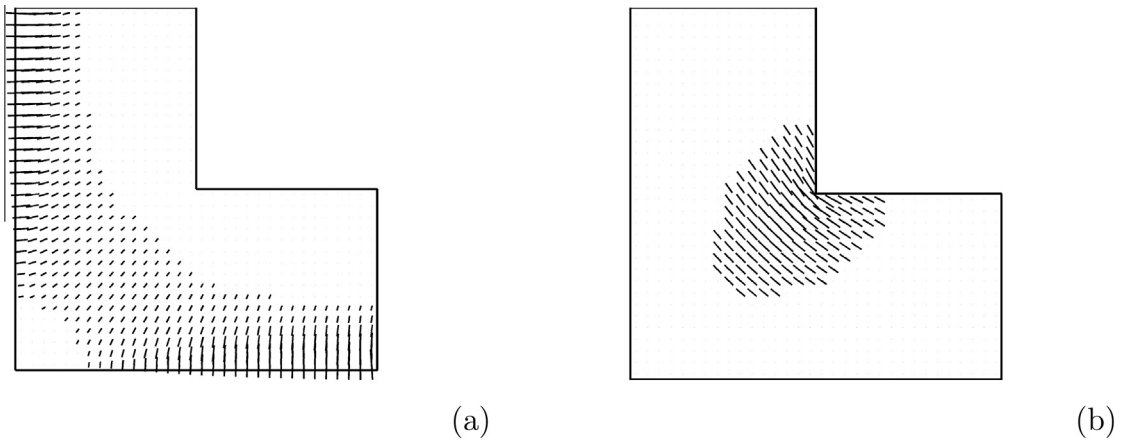

Fig. 10. Example 1. Optimal topology and orientation of the reinforcement for the cracked slab ($V_f = 0.75$): extrados (a) and intrados (b).

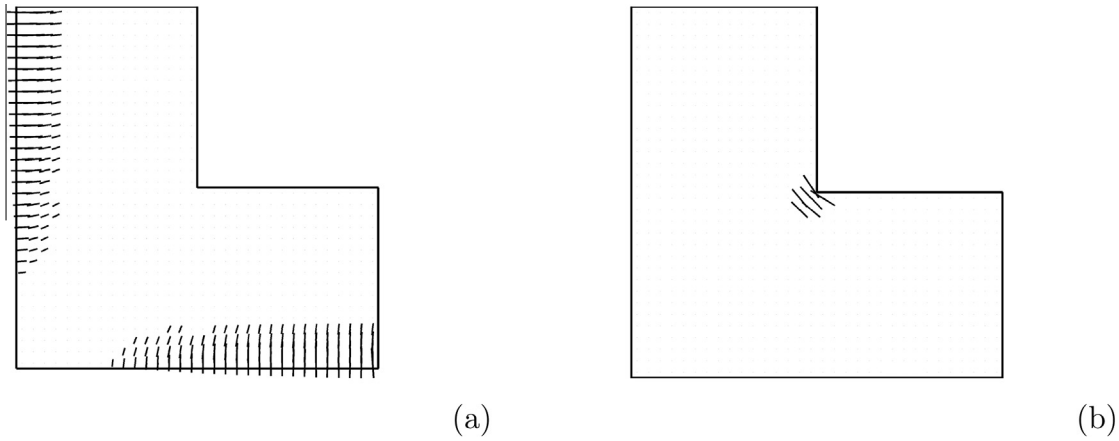

Fig. 11. Example 1. Optimal topology and orientation of the reinforcement for the cracked slab ($V_f = 0.25$): extrados (a) and intrados (b).

the following sections will be carried out accounting for a decreased stiffness, Eq. (9), with the aim of taking the effects of cracking, which affects most of the existing structures, into account.

Finally, Fig. 12 shows non-dimensional history plots of the evolving strain energy for the four cases considered so far. All of them are smooth, confirming that the penalization strategy introduced in Section 3.2 has minor effects on the convergence rate.

4.2. Example 2. Clamped square plate

Consider the square plate of Fig. 2(2), which is fully clamped along the four edges. In the uncracked plate, the maximum hogging moments act at the middle of the edges, whereas the maximum sagging moment acts at the center of the plate. A reduced moment of inertia is computed according to Eq. (9), and the ensuing principal moments are represented in Figs. 13 and 14. Comparing the fourth and the fifth line of Table 1, when passing from the uncracked to the cracked plate a change in terms of maximum moments is observed, similar to that recorded in the previous example. In fact, $M^c_{-,u}$ sensibly decreases, whereas $M^c_{+,u}$ slightly increases. The contours of the principal moments in the cracked concrete plate are shown in Fig. 14: the highest hogging and sagging moments are found to be widespread over regions larger than those in which the moments attain their peak values in the uncracked analysis.

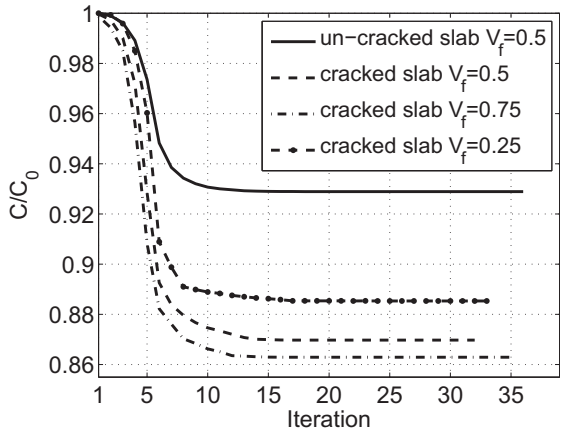

Fig. 12. Example 1. History plot of the non-dimensional compliance for different optimization settings.

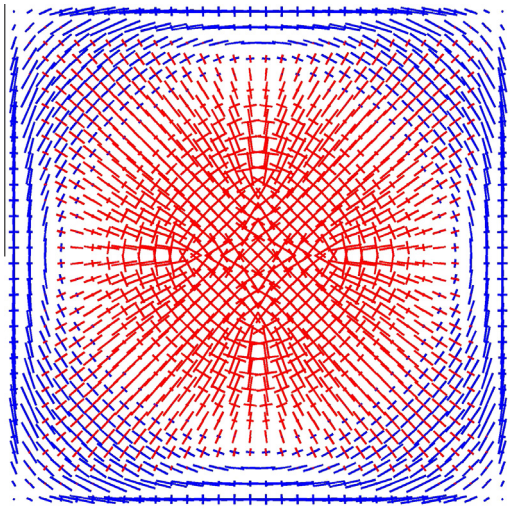

Fig. 13. Example 2. Principal moment directions in the unreinforced cracked concrete plate. Red vectors stand for sagging (positive) moments, whereas blue vectors stand for hogging (negative) moments. (For interpretation of the references to color in this figure legend, the reader is referred to the web version of this article.)

Minimizing the overall strain energy of the plate reinforced by FRPs, a solution is found in which the stiffness is increased by distributing strengthening material where the highest tensile stresses arise at either side of the plate. This provides the expected relieve of the moments acting in the concrete layer, as reported in the fifth line of Table 1. A very simple reinforcement layout can be derived from Figs. 15 and 16, which show the element-wise distribution and orientation of the FRP layers, respectively. At the extrados, a set of FRP strips sharing the same length, with fibers nearly orthogonal to the clamped edges, should be arranged along the edges, except for the small corner regions. In the central part of the intrados, FRP strips should be placed at 45°, with fibers perpendicular to the diagonals of the plate, in full agreement with the directions of the principal moments shown in Fig. 13. It is worth remarking that the FRP strips have to overlap in the central region of the extrados, which is compatible with the number of reinforcing layers ($K = 4$) chosen in Section 3.2.

In Fig. 2(2) the yield lines causing collapse of the concrete plate are also represented. The smallest load providing a rigid-plastic failure mechanism of the unreinforced structure is found if four hogging plastic hinges open along the clamped edges, and two sagging plastic hinges activate along the diagonals. The pictures in

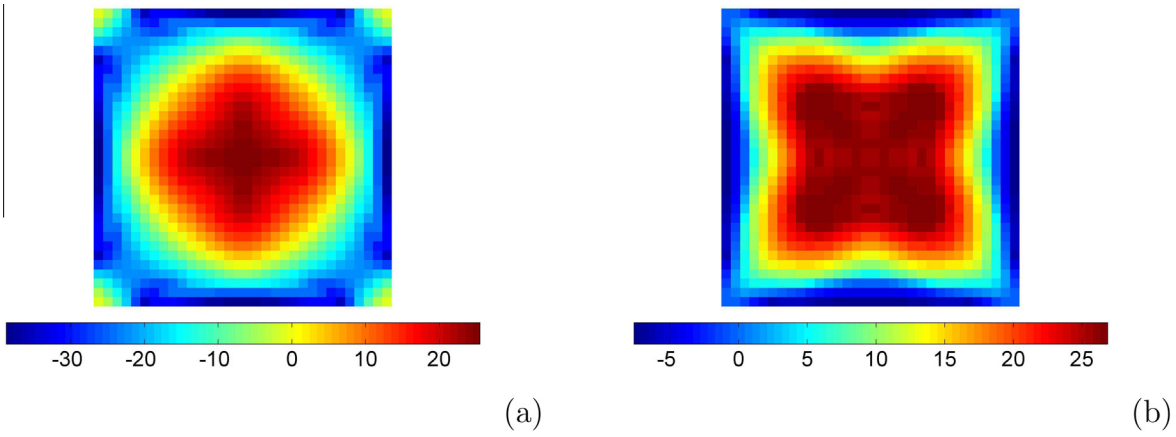

Fig. 14. Example 2. Principal moments in the unreinforced cracked concrete plate: M_I(a) and M_{II}(b), with $M_I \leqslant M_{II}$.

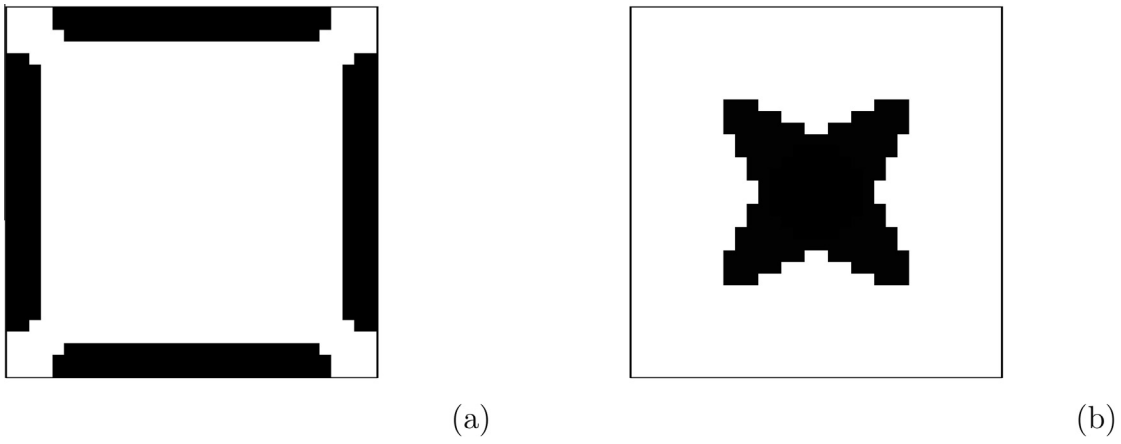

Fig. 15. Example 2. Optimal layout of the reinforcement for the cracked plate: extrados (a) and intrados (b).

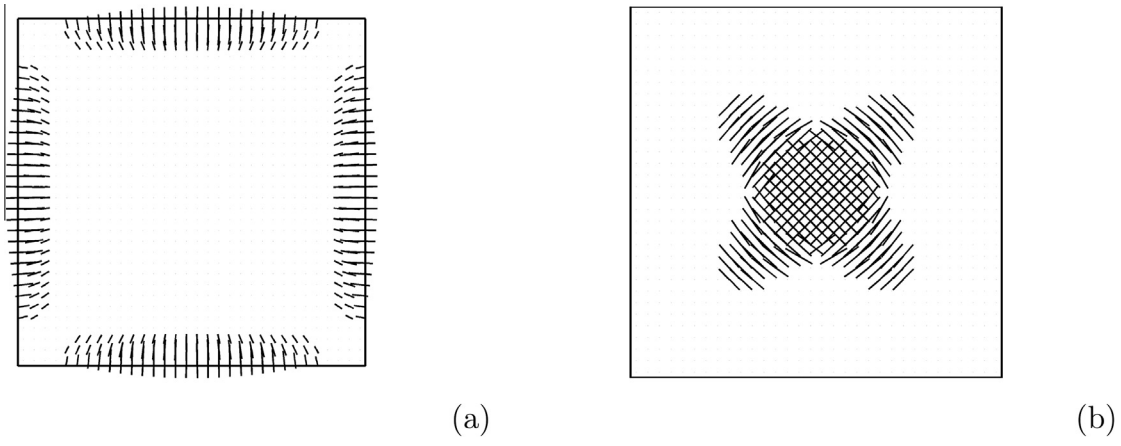

Fig. 16. Example 2. Optimal orientation of the fibers in the reinforcement of Fig. 15 for the cracked plate: extrados (a) and intrados (b).

Fig. 16 clearly show that the optimal FRP strips are arranged perpendicularly to the plastic hinges, thus resisting their opening. Note however that in the vicinity of the corners the correct layout of the yield lines is not as simple as that shown in Fig. 2(2) (Quintas, 2003).

Discrete formulations for the optimal distribution of isotropic/orthotropic material are well-known to be affected by numerical instabilities, such as mesh-dependency and checkerboard effects, see e.g. Bendsøe and Sigmund (2003), Sigmund and Petersson (1998) and Guest et al. (2004). Reinforcement problems for in-plane loaded structures have already been investigated using topology optimization techniques, showing that only minor differences are expected to arise comparing results for different mesh densities, see in particular Bruggi and Taliercio (2013). For out-of-plane loaded structures, the robustness of the proposed numerical approach is tested comparing results achieved through two different discretizations of the clamped plate of Fig. 2(2). Fig. 15 shows the optimal design obtained with 1024 elements,

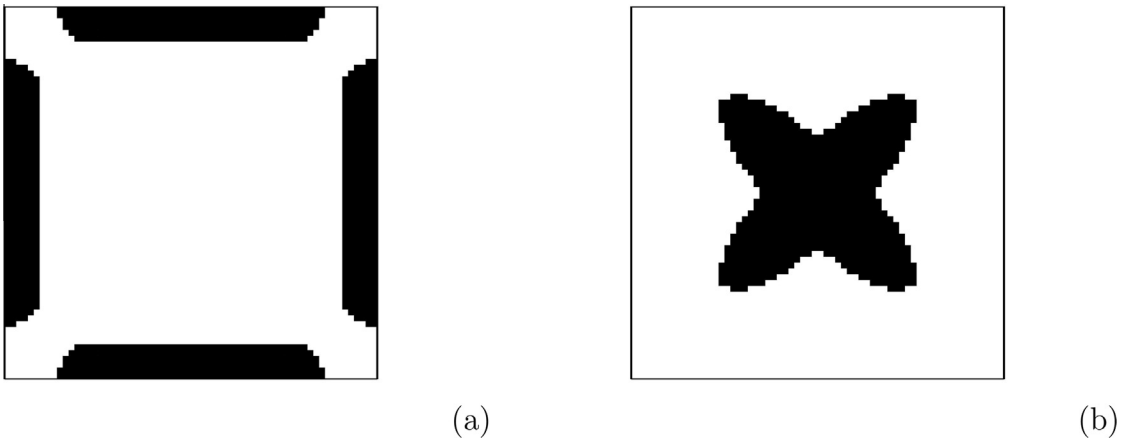

Fig. 17. Example 2. Optimal layout of the reinforcement for the cracked plate ($N = 4096$): extrados (a) and intrados (b).

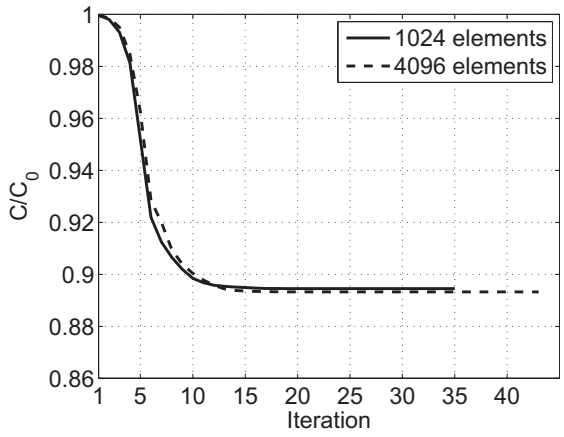

Fig. 18. Example 2. History plot of the non-dimensional compliance for different levels of refinement of the finite element mesh.

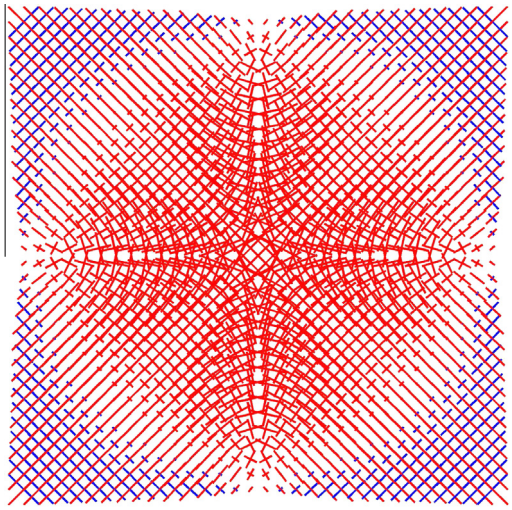

Fig. 19. Example 3. Principal moment directions in the unreinforced cracked concrete plate. Red vectors stand for sagging (positive) moments, whereas blue vectors stand for hogging (negative) moments. (For interpretation of the references to color in this figure legend, the reader is referred to the web version of this article.)

whereas Fig. 17 refers to a mesh made of 4096 elements. The optimal reinforcement layouts are almost identical, and no numerical instability arises in the computations performed with the finer mesh. Fig. 18 shows that the optimizer founds convergence virtually at the same value of the strain energy, and smoothness of the curve is preserved regardless of the level of mesh refinement.

4.3. Example 3. Simply supported square plate

The third example deals with the square plate of Fig. 2(3), which is simply supported along the four edges. Fig. 19 shows the principal directions of moments in the concrete plate, as computed according to the stiffness penalization of Eq. (9). Maximum sagging moments arise along the diagonals of the plate, whereas hogging moments are found next to the corner regions, see also Fig. 20.

The optimal design achieved through Eq. (12) is represented in Fig. 21. Most of the strips are arranged to relieve sagging moments. At the intrados, a set of FRP strips of the same orientation is distributed along the diagonals, with fibers orthogonal to them, except for the central region of the plate, which remains unreinforced. Although the positive moments are not constant along the diagonals, the reinforcing strips have approximately the same length over the whole intrados of the plate. Fibers cross the hinge of the collapse mechanism made of sagging yield lines represented in Fig. 2(3). At the extrados, a limited amount of fibers is distributed next to the corners, oriented along the diagonals. This allows the maximum negative moment M^c_-, which arises because of the so-called "corner lever" phenomenon (Wood, 1961), to be remarkably reduced. "Corner lever" affects simply supported two-way plates, in which the yield lines split at the corners as depicted in Fig. 22. Splitting is related to a hogging yield line, which crosses the corner diagonally and "levers" against the corner reaction, i.e. the holding down force. For a square plate, this phenomenon remarkably affects the geometry of the sagging yield lines, as it was found that $L_1 = 0.159L$ and $L_2 = 0.523L$, being L the length of the edge of the plate.

The optimal distribution of reinforcement represented in Fig. 21 effectively resists the collapse mechanism of the unreinforced plate, accounting for the "corner lever" phenomenon as well. The FRP strips at the extrados of the four corners intercept the hogging yield lines, whereas effectiveness of the fibers at the extrados has already been commented on. Reference is made to the sixth and seventh line of Table 1 to assess the performances of the achieved reinforcement pattern.

4.4. Example 4. Plate on walls and columns

A final example is presented to point out that the proposed numerical procedure can virtually deal with the optimization of

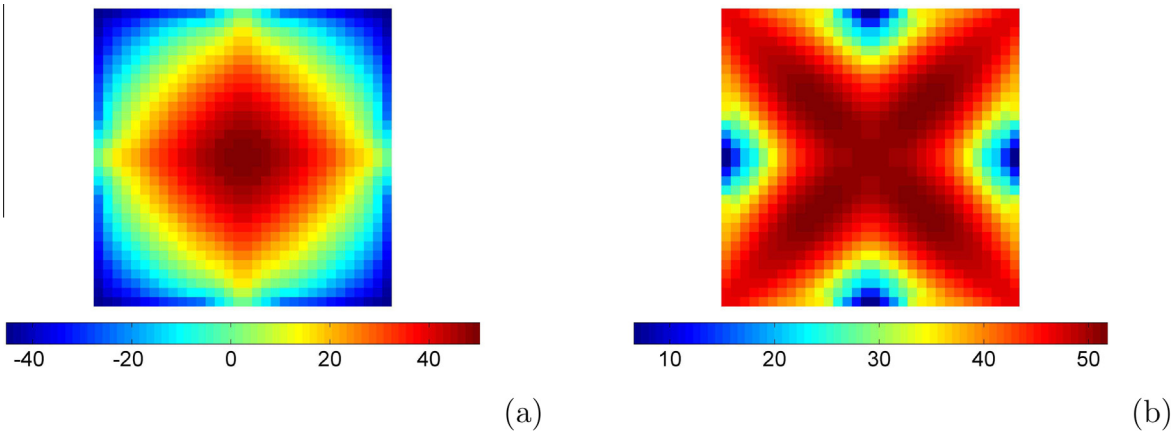

Fig. 20. Example 3. Principal moments in the unreinforced cracked concrete plate: M_I(a) and M_{II}(b), with $M_I \leqslant M_{II}$.

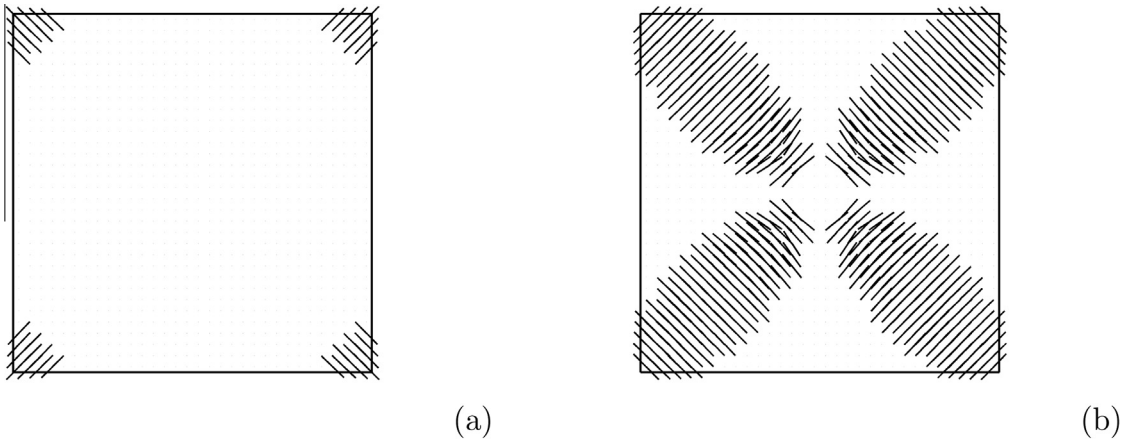

Fig. 21. Example 3. Optimal layout and orientation of the reinforcement for the cracked plate: extrados (a) and intrados (b).

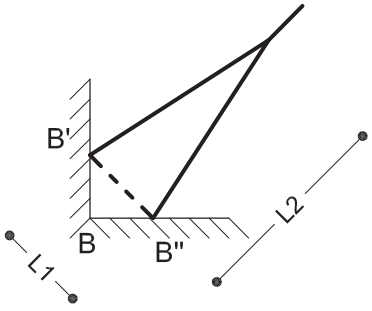

Fig. 22. Example 3. Yield lines split at internal corners due to the "corner lever" phenomenon. According to Wood (1961), $L1 = 0.159L$ and $L2 = 0.523L$ (L = length of the edge of the plate).

the fiber-reinforcement of plates of any geometry, subjected to any load and boundary conditions. Focusing on this last issue, a square plate with line and point constraints is considered (see Fig. 2(4)). The structure is simply supported along the edges $\overline{AB}$ and $\overline{BC}$, and clamped over two pillars of square section, with sides 0.5 m long, located at points D and E.

A vector map of the principal moments is represented in Fig. 23, as computed implementing the reduced effective moment of inertia I_e of Eq. (9). The highest sagging moments $M^c_{+,u}$ are found in the central region of the plate, whereas the highest negative moments $M^c_{-,u}$ arise along the line $\overline{DE}$ that connects the pillars: their values are reported in the eighth line of Table 1.

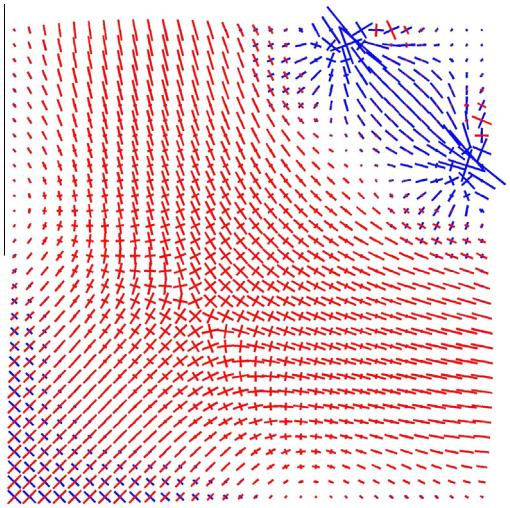

Fig. 23. Example 4. Principal directions of moments in the unreinforced cracked concrete plate. Red vectors stand for sagging (positive) moments, whereas blue vectors stand for hogging (negative) moments. (For interpretation of the references to color in this figure legend, the reader is referred to the web version of this article.)

The achieved optimal design is represented in Fig. 24. Most of the reinforcement is distributed at the intrados according to an arch-shaped layout consisting of FRP strips that approximately

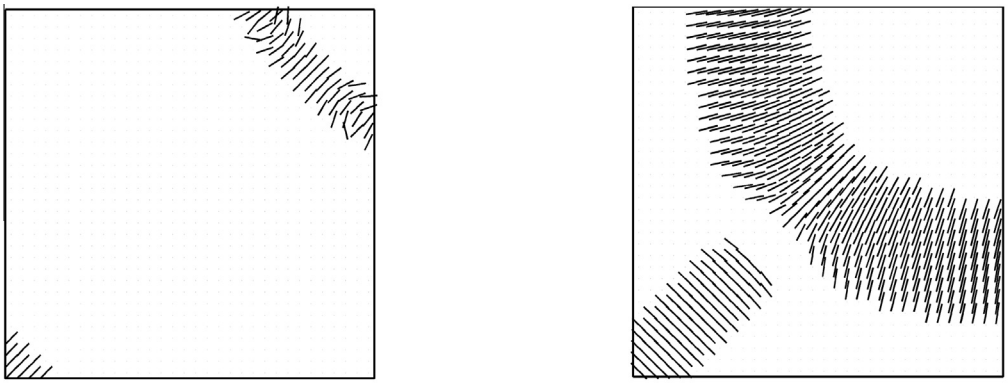

Fig. 24. Example 4. Optimal layout and orientation of the reinforcement for the cracked plate: extrados (a) and intrados (b).

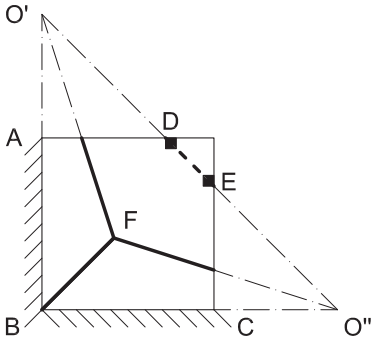

Fig. 25. Example 4. Simplified yield line pattern along with construction lines.

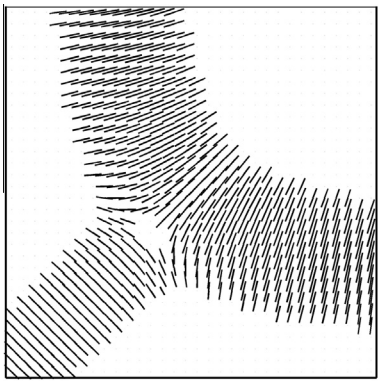

Fig. 26. Example 4. Optimal layout and orientation of the reinforcement for the cracked plate in case of extrados not attainable.

share the same length. The fibers have variable orientation, depending on the effective span between the simply supported edges and the stiff axis $\overline{DE}$ between the pillars. The extrados is reinforced by strips perpendicular to $\overline{DE}$, whereas some material is used to strengthen the perimeter of the columns. Additionally, the corner B is reinforced at both sides in a way similar to that obtained at the corners of the simply supported plate of Example 3.

In Fig. 25 the yield lines that characterize the collapse mechanism of the plate are shown in more detail. In the definition of the collapse mechanism, one has to take into account that the supported edges ($\overline{AB}$ and $\overline{BC}$) are axes of rotation, whereas the negative (sagging) yield line passes over the columns ($\overline{DE}$). Since the yield lines between adjacent rigid regions must go through the point of intersection of the axes of rotation of those regions, the three positive yield lines converging in F have to pass through the points $B, O\prime$ and O'' shown in Fig. 25. Point F lies along the diagonal of the square plate due to symmetry reasons. The length of $\overline{BF}$ could be computed minimizing the kinematic load multiplier with respect to the position of F. This was not done in the present work, but it can be easily noticed that the layout of the achieved optimal reinforcement is such as to intercept all the yield lines of the possible collapse mechanism, for a wide range of positions of point F. This remark is in full agreement with those made in the previous examples.

A final investigation is performed with reference to the plate of Fig. 2(4), but assuming that the fiber-reinforcement can be placed only at the intrados. This is a situation commonly encountered in the rehabilitation of multi-storey buildings, as usually ceilings are attainable whereas floors are not. For the same amount of material used in Fig. 24(b), the optimal distribution of fibers distributed over the available surface is shown in Fig. 26. The two layouts are very similar. The length of the strips in the arch-shaped

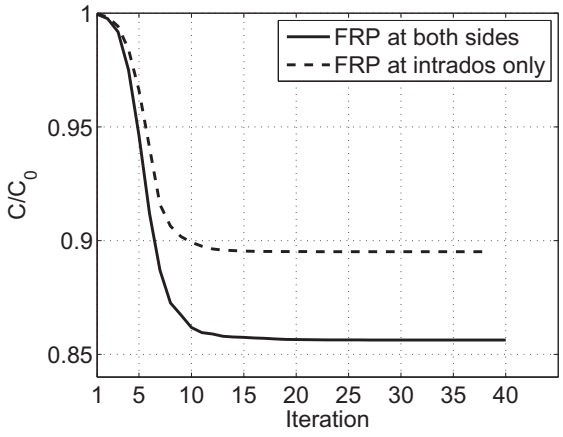

Fig. 27. Example 4. History plot of the non-dimensional compliance for the optimal layouts in Figs. 24 and 26.

topology increases, whereas more strips are added along the sagging yield line $\overline{BF}$.

The last two lines of Table 1 show the differences, in terms of performances, between the two layouts. Although the two-side reinforcement is much more efficient (allowing a decrease of nearly -15% in terms of v and M^c_+, and of more than -20% in terms of M^c_-), the intrados-only reinforcement allows the compliance and the maximum sagging moments to decrease of nearly -10%, and the negative moments to be slightly relieved. An

ultimate limit state analysis would be required to assess the enhancement in mechanical performances achieved by the proposed solutions more significantly.

Fig. 27 shows the history plots of the non-dimensional compliance during the iterative procedure that led to the results already presented in Figs. 24 and 26. The number of available layers and their location do not remarkably affect the rate and smoothness of convergence of the proposed algorithm.

5. Conclusions

A numerical procedure has been proposed to obtain the optimal layout of unidirectional and unilateral (no-compression) fiber-reinforced layers for concrete plates in bending. A volume-constrained optimization procedure has been presented, which searches for the topology and the orientation of the fiber reinforcement that minimize the strain energy of the arising composite structure. The anisotropic reinforcing layers are placed on both sides of the plate: the number of layers and the orientation of the fibers in the different layers at the extrados and at the intra-dos are completely independent. An efficient penalization scheme has been implemented in the volume-constrained formulation of the topology optimization problem to get rid of any compressive stress arising along the fibers of the FRP layers without resorting to more demanding stress-based approaches.

Numerical simulations have been carried out to assess the capabilities of the method in defining the optimal design of the fiber-reinforcement for two-way plates with different geometry and boundary conditions. As expected, different layouts of tensile-only FRP strips are achieved at the extrados and at the intra-dos. At both sides, the unilateral reinforcement is basically aligned with the direction of the principal tensile stress, which, in turn, is orthogonal to the directions of the principal moments. Note that this is consistent with the optimal retrofitting of deteriorated win-dowed walls according to the "refined method" proposed by Li et al.(2013). No checkerboard effect or significant mesh-dependency have been observed in the numerical applications.

In the numerical investigations, the effect of cracking has been considered by taking into account a reduced moment of inertia of the concrete section, as prescribed by technical codes. Redistribution of moments with respect to the uncracked scenario is found to affect the achieved optimal topology, in terms of extension of the reinforced areas and proportion of reinforcement at the intrados and at the extrados of the plate.

The distribution and the orientation of the fibers in the optimal layout was found to be such as to prevent the opening of the yield lines predicted by a limit analysis of the unreinforced plate, as the FRP strips cross the plastic hinges of the collapse mechanism and provide a resisting moment thanks to their lever arm.

Designers can exploit the output of the topology optimization procedure to define the real layout to be realized in practice, by simplifying the theoretical layout according to their engineering sense.

The ongoing research will be mainly focused on the introduction of constraints on the moment field, having the aim of achieving layouts such as to control possible stress peaks. The anisotropic modeling of the underlying reinforced concrete layer will be investigated as well.

References

ACI Committee, 2002. Building code requirements for reinforced concrete and commentary, ACI 318–02/ACI 318R–02, American Concrete Institute, Detroit.

Ananiev, S., 2005. On equivalence between optimality criteria and projected gradient methods with application to topology optimization problem. Multibody. Syst. Dyn. 13 (1), 25–38.

Arduini, M., Nanni, A., 1997. Behavior of precracked r.c. beams strengthened with carbon FRP sheets. ASCE-J. Compos. Constr. 1, 63–70.

Bai, J., 2013. Advanced Fibre-Reinforced Polymer (FRP) Composites for Structural Applications. Woodhead Publishing, Cambridge (UK).

Bakis, C.E., Bank, L.C., Brown, V.L., Cosenza, E., Davalos, J.F., Lesko, J.J., Machida, A., Rizkalla, S.H., Triantafillou, T.C., 2002. Fiber-reinforced polymer composites for construction – State-of-the-art review. J. Compos. Constr. 6, 73–87.

Bendøse, M., Kikuchi, N., 1988. Generating optimal topologies in structural design using a homogenization method. Comput. Methods Appl. Mech. Eng. 71, 197–224.

Bendøse, M., Olhoff, N., Sokolowski, J., 1985. Sensitivity analysis of problems of elasticity with unilateral constraints. J. Struct. Mech. 13 (2), 201–222.

Bendøse, M., Sigmund, O., 1999. Material interpolation schemes in topology optimization. Arch. Appl. Mech. 69, 635–654.

Bendøse, M., Sigmund, O., 2003. Topology Optimization – Theory, Methods and Applications. Springer, Berlin.

Brown, D.L., Berman, J.W., 2010. Fatigue and strength evaluation of two glass fiber-reinforced polymer bridge decks. ASCE J. Bridge Eng. 15 (3), 290–301.

Bruggi, M., 2010. On the automatic generation of strut and tie patterns under multiple load cases with application to the aseismic design of concrete structures. Adv. Struct. Eng. 13, 1167–1181.

Bruggi, M., 2014. Finite element analysis of no-tension structures as a topology optimization problem. Struct. Multi. Optim. 50 (6), 957–973.

Bruggi, M., Duysinx, P., 2013. A stress-based approach to the optimal design of structures with unilateral behavior of material or supports. Struct. Multi. Optim. 48 (2), 311–326.

Bruggi, M., Milani, G., Taliercio, A., 2013. Design of the optimal fiber-reinforcement for masonry structures via topology optimization. Int. J. Solids Struct. 50 (13), 2087–2106.

Bruggi, M., Milani, G., Taliercio, A., 2014. Simple topology optimization strategy for the FRP reinforcement of masonry walls in two-way bending. Comput. Struct. 138, 86–101.

Bruggi, M., Taliercio, A., 2013. Topology optimization of the fiber-reinforcement retrofitting existing structures. Int. J. Solids Struct. 50, 121–136.

Cheng, G.D., Guo, X., 1997. ε-relaxed approach in topology optimization. Struct. Optim. 13, 258–266.

Cheng, H.C., Kikuchi, N., 1994. An improved approach for determining the optimal orientation of orthotropic material. Struct Optim 8, 101–112.

Chen, J.F., Teng, J.G., 2001. Anchorage strength models for FRP and steel plates bonded to concrete. J. Struct. Eng. 127, 784–791.

Cunha, J., Chaves, L.P., 2014. The use of topology optimization in disposing carbon fiber-reinforcement for concrete structures. Struct. Multi. Optim. 49 (6), 1009–1023.

Duysinx, P., Bendse, M.P., 1998. Topology optimization of continuum structures with local stress constraints. Int. J. Numer. Methods Eng. 43, 1453–1478.

El Maaddawy, T., Sherif, S., 2009. FRP composites for shear strengthening of reinforced concrete deep beams with openings. Compos. Struct. 89, 60–69.

Eschenauer, H.A., Olhoff, N., 2001. Topology optimization of continuum structures: a review. Appl. Mech. Rev. 54, 331–389.

EN 1992-1-1, 2004. Eurocode 2: Design of concrete structures – Part 1-1: General rules and rules for buildings.

Garcia, R., Hajirasouliha, R., Pilakoutas, K., Guadagnini, R., Chaudat, T., 2010. Seismic strengthening of deficient RC buildings using externally bonded FRPs. In: Proc. 14th European Conference on Earthquake Engineering, Ohrid, paper n. 890 (CD ROM).

Gilbert, R.I., 1999. Deflection calculation for reinforced concrete structures – why we sometimes get it wrong. ACI Struct. J. 96 (6), 1027–1032.

Guest, J., Prevost, J., Belytschko, T., 2004. Achieving minimum length scale in topology optimization using nodal design variables and projection functions. Int. J. Numer. Methods Eng. 61, 238–254.

Hadi, M.N.S., 2003. Retrofitting of shear failed reinforced concrete beams. Compos. Struct. 62, 1–6.

Haftka, R.T., Gürdal, Z., 1992. Elements of Structural Optimization, Third Revised and Expanded Edition. Kluwer Academic publishers, Dordrecht.

Ji, J., Ding, X., Xiong, M., 2014. Optimal stiffener layout of plate/shell structures by bionic growth method. Comput. Struct. 135, 88–99.

Johansen, K.W., 1962. Yield-line theory, Cement and Concrete Association, 1962.

Kennedy, C., Goodchild, C.H., 2003. Practical Yield Line Design. The concrete center, Camberley.

Krevaikas, T.D., Triantafillou, T.C., 2005. Computer-aided strengthening of masonry walls using fibre-reinforced polymer strips. Mater. Struct. 38, 93–98.

Krog, L.A., Olhoff, N., 1999. Optimum topology and reinforcement design of disk and plate structures with multiple stiffness and eigenfrequency objectives. Comput. Struct. 72 (4–5), 535–563.

Lam, Y.C., Santhikumar, S., 2003. Automated rib location and optimization for plate structures. Struct. Multi. Optim. 25 (1), 35–45.

Li, B., Lim, C.L., 2010. Tests on seismically damaged reinforced concrete structural walls repaired using fiber-reinforced polymers. ASCE-J. Compos. Constr. 14, 597–608.

Li, B., Qian, K., Tran, C.T.N., 2013. Retrofitting earthquake-damaged RC structural walls with openings by externally bonded FRP strips and sheets. ASCE-J. Compos. Constr. 17 (2), 259–270.

Li, Q., Steven, G.P., Xie, Y.M., 1999. On equivalence between stress criterion and stiffness criterion in evolutionary structural optimization. Struct. Optim. 18, 67–73.

Liang, Q.Q., Steven, G.P., 2002. A performance-based optimization method for topology design of continuum structures with mean compliance constraints. Comput. Methods Appl. Mech. Eng. 191, 1471–1489.
Liang, Q.Q., Xie, Y.M., Steven, G.P., 1999. Optimal selection of topologies for the minimum-weight design of continuum structures with stress constraints. Proc. Inst. Mech. Eng. J. Mech. Eng. Sci. Part C 213, 755–762.
Liang, Q.Q., Xie, Y.M., Steven, G.P., 2000. Topology optimization of strut-and-tie models in reinforced concrete structures using an evolutionary procedure. ACI Struct. J. 97, 322–330.
Liang, Q.Q., Xie, Y.M., Steven, G.P., 2001. Generating optimal strut-and-tie models in prestressed concrete beams by performance-based optimization. ACI Struct. J. 98, 226–232.
Mohammed, B.S., Ean, L.W., Hossain, K.M.A., 2010. CFRP composites for strengthening of reinforced concrete walls with openings. Int. J. Eng. Res. Appl. 1, 1841–1852.
Norris, T., Saadatmanesh, H., Eshani, M.R., 1997. Shear and flexural strengthening of r/c beams with carbon fibers sheets. ASCE-J. Struct. Eng. 123, 903–911.
Paterson, J., Mitchell, D., 2003. Seismic retrofit of shear walls with headed bars and carbon fiber wrap. ASCE-J. Struct. Eng. 129, 606–614.
Pedersen, N., 1989. On optimal orientation of orthotropic materials. Struct. Optim. 1, 101–106.
Petrou, M., Parler, D., Harries, K., Rizos, D., 2008. Strengthening of reinforced concrete bridge decks using carbon fiber-reinforced polymer composite materials. ASCE J. Bridge Eng. 13 (5), 455–467.
Pisani, M.A., 2006. Evaluation of bending strength of RC beams strengthened with FRP sheets. J. Compos. Constr. 10, 313–320.
Quintas, V., 2003. Two main methods for yield line analysis of slabs. ASCE J. Eng. Mech. 129 (2), 223–231.
Rozvany, G.I.N., 1998. Exact analytical solutions for some popular benchmark problems in topology optimization. Struct. Optim. 15, 42–48.
Shahawya, M., Mirmiranb, A., Beitelman, T., 2000. Tests and modeling of carbon-wrapped concrete columns. Compos. Part B 31, 471–480.
Sigmund, O., Petersson, J., 1998. Numerical instabilities in topology optimization: a survey on procedures dealing with checkerboards, mesh-dependencies and local minima. Struct. Optim. 16, 68–75.
Svanberg, K., 1987. Method of moving asymptotes – a new method for structural optimization. Int. J. Numer. Methods Eng. 24, 359–373.
Täljsten, B., 2003. Strengthening concrete beams for shear with CFRP sheets. Constr. Build. Mater. 17, 15–26.
Triantafillou, T.C., 1998. Shear strengthening of reinforced concrete beams using epoxy-bonded FRP composites. ACI-Struct. J. 95, 107–115.
Van Den Einde, L., Zhao, L., Seible, F., 2003. Use of FRP composites in civil structural applications. Constr. Build. Mater. 17 (6–7), 389–403.
Victoria, M., Querin, Q.M., Marti, P., 2011. Generation of strut-and-tie models by topology design using different material properties in tension and compression. Struct. Multi. Optim. 44, 247–258.
Wood, R.H., 1961. Plastic and Elastic Design of Slabs and Plates with Particular Reference to Reinforced Concrete Floor Slabs. Thames and Hudson, London.